GPS Solutions (2023) 27:25
https://doi.org/10.1007/s10291-022-01363-8

ORIGINAL ARTICLE

On the potential of undifferenced and uncombined GNSS time and frequency transfer with integer ambiguity resolution and satellite clocks estimated

Xiaolong Mi[1] · Baocheng Zhang[2,5] · Ahmed El-Mowafy[1] · Kan Wang[3,4] · Yunbin Yuan[2]

Received: 9 June 2022 / Accepted: 2 November 2022 / Published online: 23 November 2022

Abstract

The use of global navigation satellite systems (GNSS) has been a competitive way to provide high-precision and low-cost time and frequency transfer results. However, the traditional GNSS method, the precise point positioning (PPP), is usually based on the ionosphere-free (IF) combination, which is not flexible when applying multi-frequency scenarios. In addition, PPP relies on precise satellite clock products with an accuracy of tens of picoseconds, limiting the time and frequency transfer performance. More importantly, achieving integer ambiguity resolution (IAR) is challenging, which makes high-precision phase observations underutilized. To achieve a better time transfer performance, we must consider all those factors from the GNSS end. In this contribution, a new GNSS time and frequency model at the undifferenced and uncombined (UDUC) level is first derived. In the UDUC model, the satellite clocks are estimated together with other parameters, and the integer ambiguities are resolved in the double-differenced (DD) form for their reliable estimation. Our numerical tests suggest three major findings. First, with integer ambiguities resolved, the UDUC model with satellite clocks fixed showed a 20% to 50% improvement compared with the UDUC PPP model. Second, with IAR and satellite clocks estimated, the proposed UDUC model shows a 10%–40% improvement over the model with satellite clocks fixed. Third, with integer ambiguities resolved and satellite clocks estimated, GPS, Galileo, and BDS-3 all have the potential to achieve frequency transfer in the low-mid 10^{-17} range for averaging times within one day.

Keywords Time and frequency transfer · Global navigation satellite system (GNSS) · Integer ambiguity resolution (IAR) · Undifferenced and uncombined · Common-clock · BDS-3

Introduction

The Optical fiber, Two-Way Satellite Time and Frequency Transfer (TWSTFT), and Global Navigation Satellite System (GNSS) are three technical means of time and frequency transfer (Matsakis et al. 2014). Optical fiber has high accuracy but is expensive and its operating range is limited (Huang et al. 2016). The advantage of TWSTFT is that it utilizes the symmetry of a two-way signal propagation to achieve high precision (Fujieda et al. 2014). GNSS is currently the most widely used time transfer technology due to its simplicity and low cost (Defraigne et al. 2015; Guyennon et al. 2009). Compared with the common-view (CV) and all-in-view (AV) approaches, precise point positioning (PPP) uses phase observations and is not limited by distance, so it is widely used in the comparison of International Atomic Time (TAI) and Coordinated Universal Time (UTC) (Defraigne et al. 2013; Rose et al. 2014; Yao et al. 2015).

✉ Baocheng Zhang
b.zhang@whigg.ac.cn

1 School of Earth and Planetary Sciences, Curtin University, Perth, Australia

2 State Key Laboratory of Geodesy and Earth's Dynamics, Innovation Academy for Precision Measurement Science and Technology, Chinese Academy of Sciences, Wuhan, China

3 National Time Service Center, Chinese Academy of Sciences, Xi'an, China

4 University of Chinese Academy of Sciences, Beijing, China

5 State Key Laboratory of Satellite Navigation System and Equipment Technology, The 54th Research Institute of China Electronics Technology Group Corporation, Shijiazhuang 050081, China

Classical PPP is usually based on an ionosphere-free (IF) combination and is usually applied to dual-frequency observations (Khodabandeh and Teunissen 2016). IF PPP is favored because the ionospheric delays, which are of no interest in time and frequency transfer, are eliminated. However, only one independent parameter, the ionospheric delay, gets eliminated, while more than one observable is sacrificed (Teunissen 2020). Compared with the IF combination, one can turn to the undifferenced and uncombined (UDUC) method, which is applied using original and uncorrelated observations and thus is flexible in multi-frequency scenarios (Odijk et al. 2016; Tu et al. 2019). The UDUC method has the added advantage of flexibly imposing dynamic constraints on all parameters to strengthen the model to the best extent possible (Zhang et al. 2019).

PPP can provide the synchronization error between the receiver time and the precise satellite clock products. These products are estimated by a global network comprising hundreds of GNSS receivers (Shi et al. 2019; Zhang et al. 2011). The International GNSS Service (IGS) final satellite clock products can achieve tens of picoseconds of precision (Guo and Geng 2018), while real-time satellite clocks can only achieve sub-nanosecond (Chen et al. 2018; Huang et al. 2014). The precision of the PPP-based time and frequency transfer thus relies on the precision of the satellite clock products used. Therefore, it is difficult for PPP to achieve a time transfer of precision of higher than a few dozen picoseconds, even with the final products.

The fixed integer carrier phase ambiguity is normally not targeted in the traditional PPP (Delporte et al. 2007; Petit et al. 2014). However, to retrieve information of high precision from GNSS, the integer characteristics of phase ambiguity should be recovered. Khodabandeh and Teunissen (2018) have theoretically proved the benefit of integer ambiguity resolution (IAR) on time and frequency transfer. Petit et al. (2015) have proposed the concept of integer PPP (IPPP) and achieved IAR in time and frequency transfer by considering the fractional cycle biases (FCB) (Geng et al. 2012). However, IPPP is also dependent on external precise satellite clock products (Petit 2021), just like the PPP. In addition, IPPP is still based on the IF combination, so it is not flexible in multi-frequency scenarios.

The precision and stability of optical clocks are about two orders of magnitude higher than the best cesium atomic clocks (Nicholson et al. 2015; Schuldt et al. 2021). Such unprecedented accuracy of optical clocks increases the requirements for time and frequency transfer techniques. However, the current PPP-based time and frequency transfer techniques cannot meet the standard of optical clocks. To better understand the potential of GNSS in time and frequency, it is necessary to study the impacts of the GNSS algorithm and equipment (Yao and Levine 2016), as this will determine whether GNSS can serve the optical clocks in the future.

We propose a new time and frequency transfer model in which satellite clocks are estimated together with other parameters. The model is based on UDUC GNSS observations as they have several advantages (Odijk et al. 2017; Zhang et al. 2019). After removing the rank deficiencies, the ambiguities are presented in a double-differenced (DD) form and then fixed using IAR strategies, ensuring that high-precision carrier phase observations are efficiently utilized. The paper aims to study the impacts of IAR and the precise satellite clock product and further explores the potential of GNSS time and frequency transfer using the proposed model. To explore the time transfer potential of GNSS itself, the common-clock time links are established to free the impact of external clocks. A common-clock time link refers to a time link connected to the same external atomic clock.

The next section presents a developed time and frequency model with IAR and satellite clocks estimated (from now on referred to as SCE model). In addition, the UDUC PPP model and the UDUC model with IAR and satellite clocks fixed (SCF model in what follows) are also derived to demonstrate the advantages of IAR and satellite clocks estimation. The following section presents the time and frequency transfer results for GPS, Galileo, and BDS-3 based on time links with zero and short baselines. Finally, in the last section, we summarize our findings and give our conclusions.

Methodology

In this section, we present three variants of the GNSS time and frequency transfer model: the UDUC PPP model, the SCF model, and the SCE model. We will show the process of constructing a full-rank GNSS time and transfer model with the help of the *S*-system theory (Odijk et al. 2016).

UDUC GNSS observation equations

AS the starting point of developing the GNSS time and frequency transfer model, we first give the equations for UDUC GNSS code and phase observations, which reads

$$\begin{aligned} p^s_{r,j} &= \rho^s_r + \tau^s_r + dt_r - dt^s + \mu_j I^s_r + d_{r,j} - d^s_j + \varepsilon^s_{p,j} \\ \phi^s_{r,j} &= \rho^s_r + \tau^s_r + dt_r - dt^s - \mu_j I^s_r + \lambda_j N^s_{r,j} + \delta_{r,j} - \delta^s_j + \varepsilon^s_{\phi,j} \end{aligned} \tag{1}$$

where s, r, j represent the satellite, receiver, and frequency, respectively; $p^s_{r,j}$ and $\phi^s_{r,j}$ are the UDUC code and phase observables, respectively; ρ^s_r is the satellite-receiver range, τ^s_r is the tropospheric delay; dt_r and dt^s are the receiver and satellite clock offsets, respectively; I^s_r is the ionospheric

delay on the first frequency and $\mu_j = \lambda_j^2 \Big/ \lambda_1^2$ is the coefficient where λ_j is the wavelength on frequency j;$N_{r,j}^s$ is the undifferenced integer phase ambiguity. $d_{r,j}$ and $d_{,j}^s$ are the receiver and satellite code biases, respectively, and their counterpart $\delta_{r,j}$ and $\delta_{,j}^s$ are the receiver and satellite phase biases; $\varepsilon_{p,j}^s$ and $\varepsilon_{\phi,j}^s$ are the code and phase observation noise and miss-modeled random effects.

Model A: UDUC PPP model

Equation (1) represents a rank-deficient system, which means not all the unknowns can be solved separately, but only their linear combinations. Therefore, as the first step in constructing the full-rank model, it is necessary to identify and eliminate these rank deficiencies, which can be done using the *S*-system theory. For instance, assuming that m satellites with f frequencies are tracked, then several rank deficiencies need to be eliminated in (1) (Table 1).

As known, precise satellite clock products $d\tilde{t}^s = dt^s + d_{,IF}^s$ based on IF combination are essential for the PPP, where $d_{,IF}^s = \frac{\mu_2}{\mu_2-\mu_1} d_{,1}^s - \frac{\mu_1}{\mu_2-\mu_1} d_{,2}^s$. As such, the rank deficiencies between the receiver and satellite clocks and that between the satellite clocks, code biases, and phase biases no longer exist. Applying the *S*-system theory can solve the remaining six rank deficiencies, with the original parameters lumped to form the new estimable parameters (Mi et al. 2019; Odijk et al. 2016). Table 2 gives these estimable parameters and their interpretations in the UDUC PPP model. The tropospheric delay is solved in its original form, which is expressed as the sum of the dry and wet delays $\tau_r^s = (\tau_d)_r^s + m_r^s \tau_r$ (Boehm et al. 2006; Zhang et al. 2021). $(\tau_d)_r^s$ is the dry part, which can be corrected a priori using empirical models (Tuka and El-Mowafy, 2013). $m_r^s \tau_r$ is the wet part, which is modeled as the product of a pre-defined mapping function m_r^s and the unknown wet part of the unknown tropospheric wet zenith delay (ZWD) τ_r.

With the rank deficiencies solved, the full-rank UDUC PPP model for time and frequency transfer is expressed as

$$\begin{aligned} \tilde{p}_{r,j}^s &= \rho_r^s + m_r^s \tau_r + d\tilde{t}_r + \mu_j \tilde{I}_r^s - \tilde{d}_{r,j}^s + \varepsilon_{p,j}^s \\ \tilde{\phi}_{r,j}^s &= \rho_r^s + m_r^s \tau_r + d\tilde{t}_r - \mu_j \tilde{I}_r^s - \tilde{\delta}_{r,j}^s + \varepsilon_{\phi,j}^s \end{aligned} \tag{2}$$

where $\tilde{p}_{r,j}^s = p_{r,j}^s + d\tilde{t}^s - (\tau_d)_r^s$ and $\tilde{\phi}_{r,j}^s = \phi_{r,j}^s + d\tilde{t}^s - (\tau_d)_r^s$.

Model B: SCF model

The disadvantage of the classical PPP model with float ambiguities is that it does not take full advantage of the integer nature of phase ambiguities, which can be solved by considering common-view satellites between two receivers. Assuming the time and frequency transfer is implemented between two receivers A and B, then the satellite code and phase biases $d_{,j}^s - d_{,IF}^s - \mu_j d_{,GF}^s$ and $\delta_{,j}^s - d_{,IF}^s + \mu_j d_{,GF}^s$ are the same for the receivers A and B with the same satellites tracked. Taking some common parameters as the *S*-basis, the number of estimated parameters can be reduced, and the phase ambiguities can be

Table 2 Estimable unknown parameters and their interpretation formed by a commonly used *S*-basis in PPP (Liu et al. 2017), where $d_{r,GF} = \frac{1}{\mu_2-\mu_1}(d_{r,2} - d_{r,1})$, $d_{,GF}^s = \frac{1}{\mu_2-\mu_1}(d_{,2}^s - d_{,1}^s)$ and $d_{r,IF} = \frac{\mu_2}{\mu_2-\mu_1} d_{r,1} - \frac{\mu_1}{\mu_2-\mu_1} d_{r,2}$ (GF: geometry-free)

Estimable parameter	Notation and interpretation
Receiver clock	$d\tilde{t}_r = dt_r + d_{r,IF}$
Satellite code bias	$\tilde{d}_{r,j}^s = d_{,j}^s - d_{,IF}^s - \mu_j d_{,GF}^s - d_{r,j} + d_{r,IF} + \mu_j d_{r,GF}$; $j \geq 3$
Satellite phase bias	$\tilde{\delta}_{r,j}^s = \delta_{,j}^s - d_{,IF}^s + \mu_j d_{,GF}^s - \lambda_j N_{r,j}^s - \delta_{r,j} + d_{r,IF} - \mu_j d_{r,GF}$; $j \geq 1$
Ionospheric delay	$\tilde{I}_r^s = I_r^s + d_{r,GF} - d_{,GF}^s$
S-basis parameters	$d_{r,j}$, $\delta_{r,j}$, $d_{r,IF}$,$N_{r,j}^s$, $d_{r,GF}$, $d_{,GF}^s$

Table 1 Rank deficiencies in the UDUC GNSS observation equations, together with the sources and sizes of those rank deficiencies as presented in (1) (Odijk et al. 2016)

Type	Source of those rank deficiencies	Size
1	Between the receiver and satellite clocks	1
2	Between the receiver and satellite code biases	f
3	Between the receiver and satellite phase biases	f
4	Between the receiver clocks, code biases, and phase biases	1
5	Between the satellite clocks, code biases, and phase biases	m
6	Between the satellite phase biases and ambiguities	$f \times m$
7	Between the ionospheric delays and receiver code/phase biases	1
8	Between the ionospheric delays and satellite code/phase biases	m

constructed in the DD form, which is the most reliable form for IAR. In this situation, IAR can be realized through DD integer ambiguities, while precise external products provide satellite clocks, so this model can be called the SCF model. With IAR and satellite clocks introduced from external sources, the SCF model can be expressed as follows:

$$\begin{aligned}
\tilde{p}^s_{A,j} &= \rho^s_A + m^s_A\tau_A + d\tilde{t}_A + \mu_j\tilde{I}^s_A - \tilde{d}^s_{A,j} + \varepsilon^s_{p,j}\\
\tilde{\phi}^s_{A,j} &= \rho^s_A + m^s_A\tau_A + d\tilde{t}_A - \mu_j\tilde{I}^s_A - \tilde{\delta}^s_{A,j} + \varepsilon^s_{\phi,j}\\
\tilde{p}^s_{B,j} &= \rho^s_B + m^s_B\tau_B + d\tilde{t}_B + \mu_j\tilde{I}^s_B - \tilde{d}^s_{A,j} + \tilde{d}_{AB,j} + \varepsilon^s_{p,j}\\
\tilde{\phi}^s_{B,j} &= \rho^s_B + m^s_B\tau_B + d\tilde{t}_B - \mu_j\tilde{I}^s_B - \tilde{\delta}^s_{A,j} + \tilde{\delta}_{AB,j} + \lambda_j N^{1s}_{AB,j} + \varepsilon^s_{\phi,j}
\end{aligned} \tag{3}$$

where $\tilde{p}^s_{r,j}$ and $\tilde{\phi}^s_{r,j}$ have the same definition as given in Equation (2). The interpretation of $\tilde{d}_{AB,j}$,$\tilde{\delta}_{AB,j}$ and $N^{1s}_{AB,j}$ are given in Table 3.

Equation (3) can be defined as the ionosphere-float SCF model as no relationship is assumed between I^s_A and I^s_B in this situation. However, for baselines with less than 10 km, I^s_A and I^s_B are sufficiently correlated such that they can be considered approximately equal. In this situation, we can enhance the model strength and achieve fast IAR by considering the regional ionospheric correlation between different receivers. Note in Equation (3) that $\tilde{I}^s_r = I^s_r + d_{r,GF} - d^s_{,GF}$, which includes $d_{r,GF}$ and $d^s_{,GF}$. However, if we choose $\tilde{I}^s_A$ as S-basis, then the between-receiver ionospheric delay can be written as $\tilde{I}^s_{AB} = I^s_{AB} + d_{AB,GF}$. For short baselines less than 10 km, it is safe to assume $I^s_{AB} = 0$ (Odolinski et al. 2015; Teunissen 1997) that the between-receiver differential code bias (DCB) $d_{AB,GF}$ can be separated. This model can be defined as the ionosphere-fixed SCF model, which reads

$$\begin{aligned}
\tilde{p}^s_{A,j} &= \rho^s_A + m^s_A\tau_A + d\tilde{t}_A + \mu_j\tilde{I}^s_A - \tilde{d}^s_{A,j} + \varepsilon^s_{p,j}\\
\tilde{\phi}^s_{A,j} &= \rho^s_A + m^s_A\tau_A + d\tilde{t}_A - \mu_j\tilde{I}^s_A - \tilde{\delta}^s_{A,j} + \varepsilon^s_{\phi,j}\\
\tilde{p}^s_{B,j} &= \rho^s_B + m^s_B\tau_B + d\tilde{t}_B + \mu_j\tilde{I}^s_A + \mu_j d_{AB,GF} - \tilde{d}^s_{A,j} + \tilde{d}_{AB,j} + \varepsilon^s_{p,j}\\
\tilde{\phi}^s_{B,j} &= \rho^s_B + m^s_B\tau_B + d\tilde{t}_B - \mu_j\tilde{I}^s_A - \mu_j d_{AB,GF} - \tilde{\delta}^s_{A,j} + \tilde{\delta}_{AB,j} + \lambda_j N^{1s}_{AB,j} + \varepsilon^s_{\phi,j}
\end{aligned} \tag{4}$$

where the interpretation of the estimated parameters is given in Tables 2 and 3.

Model C: SCE model

The above two variants are free of the first and fifth types of rank deficiencies (in Table 1) with external satellite clocks fixed. However, high-precision time and frequency transfer are significantly impacted by the satellite clock products used. In this section, a time and frequency transfer model is constructed without using precise satellite clocks. For the rank deficiencies shown in Table 1 (except for the first and fifth ones), we would like to use the same S-basis with Model A and Model B. In addition, to construct DD phase ambiguities, the same S-basis are defined as Equation (3). For the new rank deficiency between the receiver and satellite clocks, the clock of receiver A is set as the S-basis. In addition, the new rank deficiencies between satellite clocks, code biases, and phase biases are eliminated by fixing the satellite IF code biases $d^s_{,IF}$ for each satellite. In this case, the satellite clocks are estimated rather than corrected by external sources, so this model can be called the SCE model. In this way, we can access the full-rank SCE model, which reads

$$\begin{aligned}
\tilde{\tilde{p}}^s_{A,j} &= \rho^s_A - d\tilde{\tilde{t}}^s + \mu_j\tilde{I}^s_A - \tilde{d}^s_{A,j} + \varepsilon^s_{p,j}\\
\tilde{\tilde{\phi}}^s_{A,j} &= \rho^s_A - d\tilde{\tilde{t}}^s - \mu_j\tilde{I}^s_A - \tilde{\delta}^s_{A,j} + \varepsilon^s_{\phi,j}\\
\tilde{\tilde{p}}^s_{B,j} &= \rho^s_B + m^s_B\tau_{AB} + d\tilde{t}_{AB} - d\tilde{\tilde{t}}^s + \mu_j\tilde{I}^s_B - \tilde{d}^s_{A,j} + \tilde{d}_{AB,j} + \varepsilon^s_{p,j}\\
\tilde{\tilde{\phi}}^s_{B,j} &= \rho^s_B + m^s_B\tau_{AB} + d\tilde{t}_{AB} - d\tilde{\tilde{t}}^s - \mu_j\tilde{I}^s_B - \tilde{\delta}^s_{A,j} + \tilde{\delta}_{AB,j} + \lambda_j N^{1s}_{AB,j} + \varepsilon^s_{\phi,j}
\end{aligned} \tag{5}$$

where $\tilde{\tilde{p}}^s_{r,j} = p^s_{r,j} - (\tau_d)^s_r$ and $\tilde{\tilde{\phi}}^s_{r,j} = \phi^s_{r,j} - (\tau_d)^s_r$. $d\tilde{\tilde{t}}^s = dt^s - dt_A + d^s_{,IF} - d_{A,IF} - m^s_A\tau_A$ is the estimable satellite clock, and the between-receiver estimable clock is formulated as $d\tilde{t}_{AB} = dt_{AB} + d_{AB,IF}$. As can be seen, without precise satellite clocks, one cannot access the receiver clock of each station, but only the between-receiver clocks. As the ionospheric delay between different receivers is not considered in such a case, this model can be defined as the ionosphere-float SCE model.

For short baselines less than 10 km, if $I^s_{AB} = 0$ is assumed, and then, we choose $\tilde{I}^s_A$ as a S-basis as in (4), the ionosphere-fixed SCE model can be constructed similar to (4) as follows,

Table 3 Estimable unknown parameters and their interpretation as well as the used S-basis in the SCF model

Estimable parameter	Notation and interpretation
Between-receiver code bias	$\tilde{d}_{AB,j}=d_{B,j} - d_{A,j} - d_{AB,IF} - \mu_j d_{AB,GF}; j \geq 3$
Between-receiver phase bias	$\tilde{\delta}_{AB,j}=\delta_{B,j} - \delta_{A,j} - d_{AB,IF} + \mu_j d_{AB,GF} + \lambda_j N^1_{AB,j}; j \geq 1$
DD phase ambiguity	$N^{1s}_{AB,j}=N^s_{AB,j} - N^1_{AB,j}$
S-basis	$\tilde{d}_{A,j}$, $\tilde{\delta}_{A,j}$, $N^1_{AB,j}$

$$\begin{aligned}
\tilde{P}^s_{A,j} &= \rho^s_A - d\tilde{t}^s + \mu_j \tilde{I}^s_A - \tilde{d}^s_{A,j} + \varepsilon^s_{p,j} \\
\tilde{\phi}^s_{A,j} &= \rho^s_A - d\tilde{t}^s - \mu_j \tilde{I}^s_A - \tilde{\delta}^s_{A,j} + \varepsilon^s_{\phi,j} \\
\tilde{P}^s_{B,j} &= \rho^s_B + m^s_B \tau_{AB} + d\tilde{t}_{AB} - d\tilde{t}^s + \mu_j \tilde{I}^s_A + \mu_j d_{AB,GF} - \tilde{d}^s_{A,j} + \tilde{d}_{AB,j} + \varepsilon^s_{p,j} \\
\tilde{\phi}^s_{B,j} &= \rho^s_B + m^s_B \tau_{AB} + d\tilde{t}_{AB} - d\tilde{t}^s - \mu_j \tilde{I}^s_A - \mu_j d_{AB,GF} - \tilde{\delta}^s_{A,j} + \tilde{\delta}_{AB,j} + \lambda_j N^{1s}_{AB,j} + \varepsilon^s_{\phi,j}
\end{aligned} \tag{6}$$

where the estimated unknowns and their interpretation are the same as in (5).

Table 4 gives a comparison of the UDUC PPP model (Model A), the SCF model (Model B), and the SCE model (Model C), for a better understanding of them.

Experimental results

This section starts with an outline of the experimental setup, including the characteristics of the experimental data sets considered for this study and our data processing strategies. Following that is an evaluation of the time and frequency transfer performance with the three models using GPS-only at two laboratories. This evaluation aims to illustrate the benefits of IAR and satellite clocks estimation by comparing the three models. Then, the potential of time and frequency performance of the SCE model using GPS, Galileo and BDS-3 is evaluated.

Experimental setup

We collected GNSS data from three laboratories, including the United States Naval Observatory (USNO), USA, the Physikalisch-Technische Bundesanstalt (PTB), Germany, and the Innovation Academy for Precision Measurement Science and Technology (APM), Chinese Academy of Sciences, China. The relevant characteristics of these experimental data sets considered for this study are shown in Table 5, including the station name, institute, reference clock, receiver and antenna type, and location of the receivers.

The first set of receivers, operated by the USNO with the same H-maser clock, create one zero baseline (USN7-USN8). We collect GPS observations at both L1 and L2 of those receivers at the USNO from August 7 to 13, 2021. At the PTB, the receivers of PTBB and PT10 are connected to the same H-maser clock, forming a short baseline, with data collection from February 4 to 10, 2022. In addition, one zero baseline (APM3-APM5) and one short baseline (APM4-APM5) are formed, which are connected to the same H-maser clock at the APM. The code and phase observations of GPS L1 + L2, Galileo E1 + E5a, and BDS-3 BIC + B2a are tracked for the three receivers at the APM. This set of experimental data corresponds to the period January 3–9, 2022.

The between-receiver single-differenced (SD) ionospheric and tropospheric delays are eliminated for the zero and short baselines; thus, the ionospheric-fixed variants of the SCF and SCE models are used. The common-clock configuration can eliminate the influence of any imprecision of the receiver clocks, making it possible to evaluate the potential of GNSS time and frequency transfer under almost ideal conditions. A bidirectional Kalman filter was used to avoid the convergence process (Liu and Zhang 2021). The precise

Table 4 The comparison of the three models developed above

Item	Model A	Model B	Model C
Observation	UDUC	UDUC	UDUC
Satellite clocks	Corrected by precise satellite clock products	Corrected by precise satellite clock products	Estimated as unknowns
Phase ambiguity	Coupled with other parameters	Integrated into a DD form, enabling IAR	Integrated into a DD form, enabling IAR
Ionospheric constraints	Not considered	Considered	Considered

Table 5 A general overview of GNSS data sets used in our analysis

Station name	Institute	Reference clock	Receiver type	Antenna type	Location
USN7	USNO	H-maser	SEPT POLARX5TR	TPSCR.G5	38.92°N, 77.7°W
USN8			SEPT POLARX5TR		
PTBB	PTB	H-maser	SEPT POLARX5TR	LEIAR25.R4	52.30°N, 110.46°E
PT10			JAVAD TRE_G3T	NAX3G + C	
APM3	APM	H-maser	SEPT POLARX5	TRM159800.00	30.53°N, 114.36°E
APM5			SEPT POLARX5		
APM4			TRIMBLE ALLOY	TRM5791.00	

Table 6 Main data processing strategies in this study for the three models

Item	Model A	Model B	Model C
Receiver clock	Estimated as white noise		
Ionospheric delays	Estimated as white noise		
Tropospheric delays	Dry delay: corrected by the UNB3m model (Leandro et al. 2008) Wet delay: estimated as a random-walk process (Hadas et al. 2017)		
Stochastic model	Elevation-dependent weighting (Shen et al. 2009) Phase and code standard deviation (STD): 0.003 m and 0.3 m		
Orbits	Precise orbits	Precise orbits	Broadcast orbits
Satellite clocks	Precise satellite clocks	Precise satellite clocks	Estimated as white noise
Satellite phase biases	Estimated as a time-constant		
Between-receiver DCB		Estimated as white noise	Estimated as white noise
Between-receiver phase biases		Estimated as a time-constant	Estimated as a time-constant
IAR		LAMBDA (Teunissen 1995) with a ratio test of a threshold of 3 (Teunissen and Verhagen 2009)	
Outlier detection and elimination	DIA (Teunissen 2018)		

satellite orbits and clocks were fixed using the IGS final products for both Models A and B, and the monthly DCBs published by the Center for Orbit Determination in Europe (CODE) were used. The main processing strategies for the three models are shown in Table 6. It should be mentioned that all models are based on in-house software, which can avoid the impact of differences in data processing strategies (such as tropospheric delay) of different software.

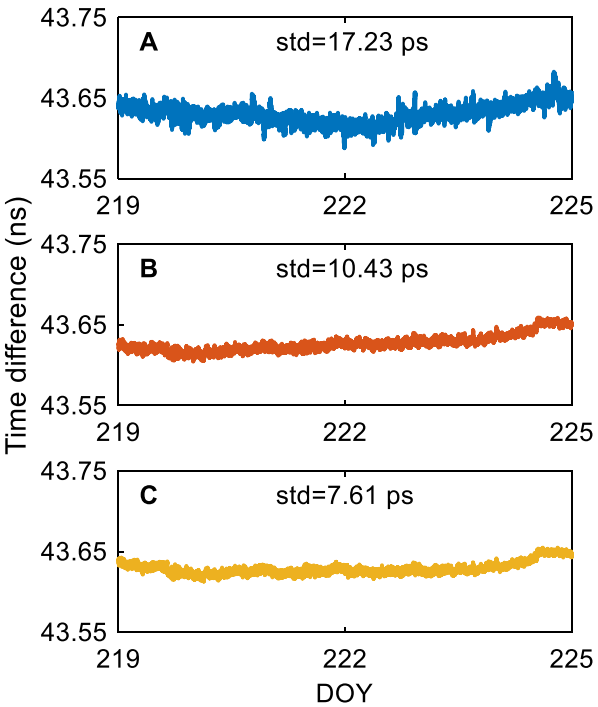

Fig. 1 Time difference between the receivers USN7 and USN8 with three different models using GPS L1/L2 observations on days of year (DOYs) 219–224, 2021

Experiments at USNO

Figure 1 shows the time difference obtained for the zero baseline USN7-USN8 using the three models discussed before. USN7 and USN8 are connected to the same H-maser clock and the same antenna; thus, the time difference is expected to be constant. Therefore, a comparison of the results can easily show which model has the best performance. We find that the STD of the time difference of the UDUC PPP model and the SCF model are 17.23 and 10.43 ps, respectively, showing an improvement of 39.5%. The benefits of the SCF model over the UDUC PPP model lie in two aspects. First, the common-view satellites are used to form the DD ambiguities to achieve IAR. Second, the ionospheric constraint is considered in the SCF model for easier IAR. The yellow curve shows that compared with the UDUC PPP model and the SCF model, the SCE model shows the smallest noise with 7.61 ps, showing 55.8 and 27.0% improvement, respectively. This shows that the use of satellite clock products does have an impact on time transfer. The advantage of the SCE model lies in that the satellite clocks are estimated synchronously with other parameters, making the model more rigorous.

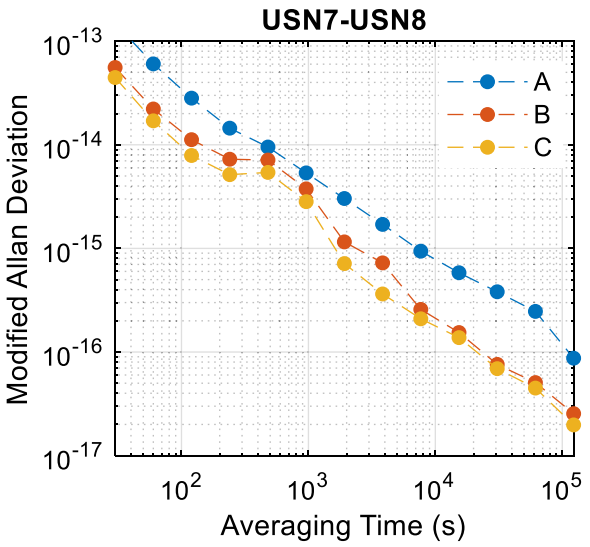

Fig. 2 MDEV of the USN7-USN8 with the PPP model (Model A), the SCF model (Model B) and the SCE model (Model C)

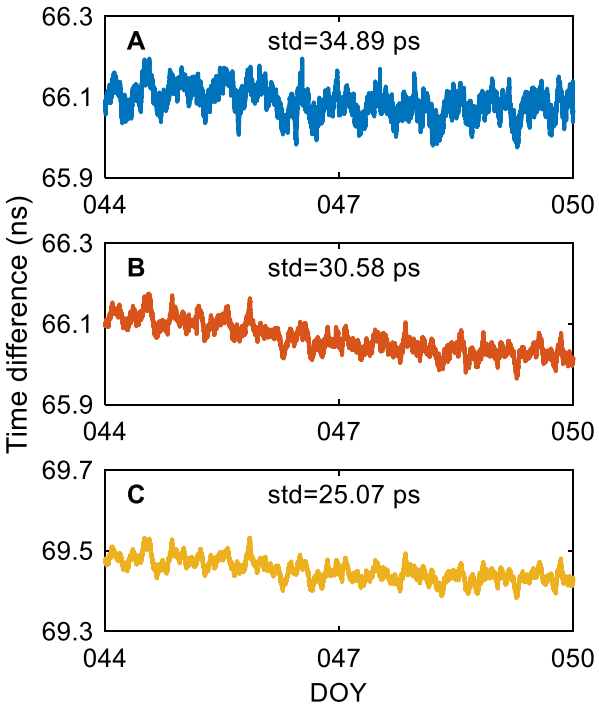

Fig. 3 Time difference between the receivers PTBB and PT10 with the three different models and GPS L1/L2 observations on DOYs 044–049, 2022

Figure 2 illustrates the modified Allan deviation (MDEV) of the time differences of the USN7-USN8. With the successful IAR, the frequency stability of the SCF model and SCE model reaches 5.6×10^{-14} and 4.5×10^{-14} for an averaging time at 30 s, respectively, while that of the UDUC PPP model can only reach 1.5×10^{-13}. The frequency stability for an averaging time at 15,360 s with the three models is 5.82×10^{-16}, 1.54×10^{-16} and 1.37×10^{-16}, respectively. Compared with the UDUC PPP model and the SCF model, the MDEV of the SCE model has improved by 76.4 and 11.0%, which shows the benefits of the IAR and satellite clocks estimation.

Experiments at PTB

The second experiment is based on the data collected at the PTB, Germany. The receivers PTBB and PT10 are connected to the same H-maser clock but with different antennas. From Fig. 3, we can see that the results from PTBB-PT10 are not as good as from USN7-USN8. This is reasonable since the antenna and receiver effects inevitably affect the time transfer performance. The corresponding STD of the time difference for the three models is 34.89, 30.58 and 25.07 ps, respectively. The STD of the SCF model improves 12.4% over the UDUC PPP model, due to the benefits of the IAR. In addition, the SCE model has gains of 28.1 and 18.0%, respectively, over the UDUC PPP model and the SCF model, showing the advantages of both IAR and satellite clocks estimation. It should be mentioned that the time difference of the UDUC PPP model and the SCF model is at the same level because the same precise satellite clock products are used. However, the situation is different for the SCE model, as only the broadcast ephemeris is used.

The MDEV of the three models for the PTBB-PT10 is shown in Fig. 4, from which we can confirm and extend

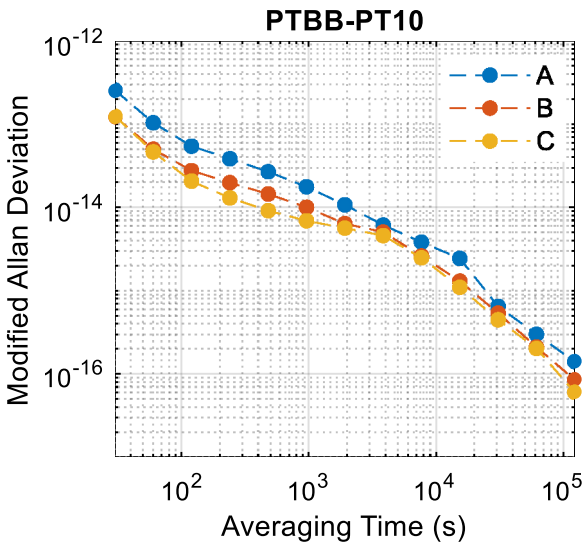

Fig. 4 MDEV of the PTBB-PT10 with the PPP model (Model A), the SCF model (Model B) and the SCE model (Model C)

our above findings. First, the SCF and the SCE models have improvements over the PPP model, as shown by its MDEV. The SCF model has an 18–52% improvement over the UDUC PPP model for averaging times at one day and below. Second, compared with the SCF model, with satellite clocks estimated together with other parameters, the SCE model can achieve better performance. For example, the frequency stability for an averaging time at one day for the two models is 6.03×10^{-17} and 8.51×10^{-17}. Compared with the SCF model, the SCE model shows an improvement of 29.0% for frequency stability, indicating the advantage of synchronously estimating satellite clocks.

Experiments at APM

From the previous experiments at USNO and PTB, the benefits of the SCE model were demonstrated using only GPS observations. In this test, using multi-GNSS data collected at the APM, the potential of time and frequency transfer performance of the proposed SCE model is evaluated using multi-GNSS.

Figure 5 depicts the time difference of the APM3-APM5 of the SCE model for GPS, Galileo, and BDS-3, from which two conclusions can be drawn. First, the time difference of APM3-APM5 for each constellation shows a trend. This is not surprising since the common-clock configuration makes

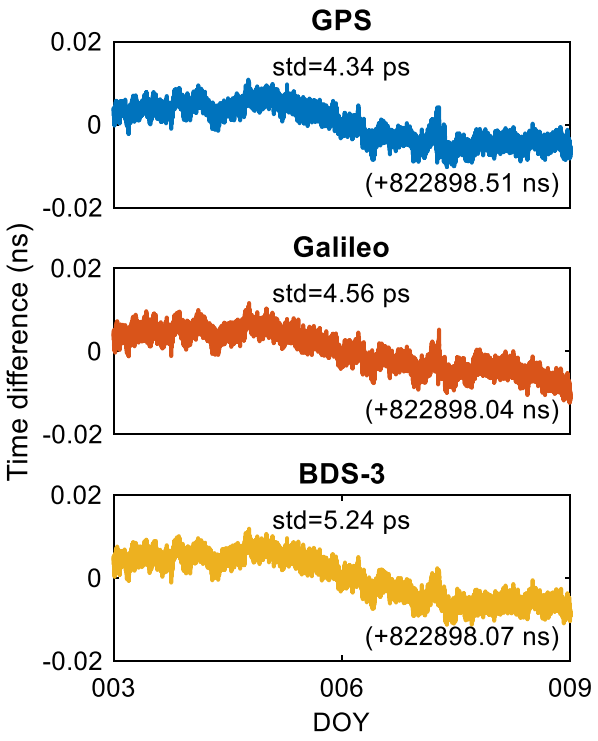

Fig. 5 Time difference between the receivers APM3 and APM5 of the SCE model for GPS, Galileo, and BDS-3 from DOYs 003–008, 2022

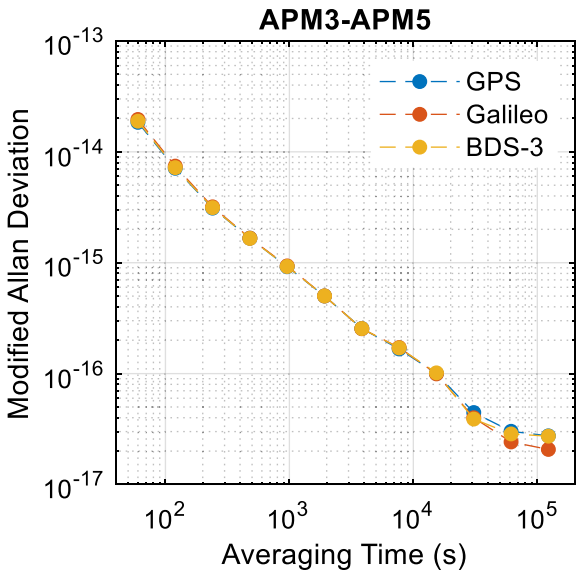

Fig. 6 MDEV of the APM3-APM5 of the SCE model for GPS, Galileo, and BDS-3 calculated from DOYs 003–008, 2022

the time transfer largely dependent on the between-receiver IF code bias ($d_{AB,IF}$). Although usually, in time transfer, it is assumed to be time invariant, this is not the case (Defraigne et al. 2021; Mi et al. 2021). The studies have shown that the receiver code bias can vary significantly, and an essential driving factor is the ambient temperature (Mi et al. 2020; Rieck et al. 2003; Zhang et al. 2020). Second, we can achieve picosecond time transfer with IAR and satellite clocks estimated for each constellation. The STD of the time difference for GPS, Galileo, and BDS-3 is 4.34, 4.56, 5.24 ps, respectively. It is worth noting that at APM3 and APM5, the same type of receiver is used and they are connected to the same H-maser clock and antenna. Thus, theoretically, this could be the limit for GNSS time transfer as the common error from receiver-end cable also be canceled. However, it can be seen from the results that the time transfer is not completely white noise because it is difficult to make the variation in the receiver bias completely consistent even with the same type of receiver (Mi et al. 2020).

Figure 6 depicts the MDEV of the APM3-APM5 time link with GPS, Galileo, and BDS-3, from which several conclusions can be drawn. First, GPS, Galileo, and BDS-3 show similar levels in terms of frequency stability. For example, the frequency stability of the APM3-APM5 with GPS, Galileo and BDS-3 is 5.01×10^{-16}, 5.01×10^{-16} and 4.81×10^{-16} for an averaging time at 1920 s. In the experiments in USNO and PTB, we demonstrate the superiority of the SCE model using GPS-only observations. Using the APM3-APM5, we find that with satellite clocks estimated and integer ambiguities resolved, Galileo and BDS-3 also have the potential to achieve 5×10^{-16} frequency transfer for averaging times

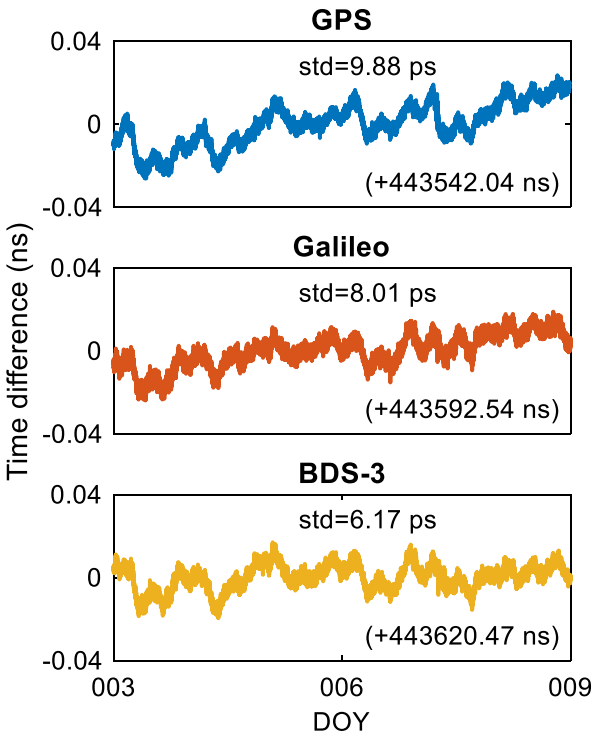

Fig. 7 Time difference between the receivers APM4 and APM5 of the SCE model for GPS, Galileo, and BDS-3 from DOYs 003–008, 2022

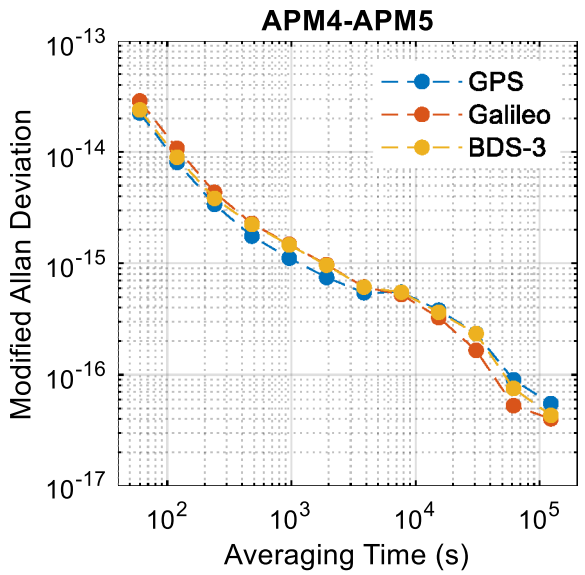

Fig. 8 MDEV of the APM4-APM5 using the SCE model for GPS, Galileo, and BDS-3 calculated from DOYs 003–008, 2022

within 30 min. The SCE model achieves such high frequency stability without reliance on precise satellite products, showing the significant benefit of the satellite clocks estimation. Second, GNSS has the potential to achieve sub-10^{-16} frequency transfer for averaging times at eight hours and above. As we can see from Fig. 6, although the performance of the three constellations is different, they can all achieve frequency transfer in the low-mid 10^{-17} range. For example, for an averaging time of one day, the frequency stability of APM3-APM5 with GPS, Galileo and BDS-3 is better than 3.01×10^{-17}, 2.41×10^{-17} and 2.85×10^{-17}, respectively.

Figures 7 and 8 show the time difference and corresponding MDEV for another baseline, APM4-APM5, with different types of receivers and antennas. The result of this time link is not as good as the APM3-APM5 with the same type of receiver and antenna, which shows the effect of receiver and antenna that must be considered. However, even in this case, GPS, Galileo, and BDS-3 can still achieve time transfer on the order of picoseconds. The STD of the time difference for GPS, Galileo, and BDS-3 are 9.88, 8.01, 6.17 ps, respectively. The time transfer results of the three constellations have different trends, which are believed to be caused by the antenna, the receiver, and the cable. Concerning the frequency stability, all three constellations can reach sub-10^{-16} for averaging times at half the day and above.

It is, however, still challenging to achieve picosecond time transfer and low-mid 10^{-17} range frequency transfer based on current atomic clocks and methods for the following reasons. First, the best H-masers are only of subnanosecond accuracy with $1-2 \times 10^{-16}$ frequency stability. Existing equipment can thus hardly reach the expected accuracy and stability. Second, the distance over which time and frequency transfer is needed is usually hundreds or even thousands of kilometers, so it is challenging to realize IAR without accurate atmospheric information. With the popularization of optical clocks and precise modeling of the atmospheric delays, it can be expected that picosecond time transfer results and sub-10^{-16} frequency transfer with GNSS will be demonstrated.

Conclusion

The development of high-precision optical clocks has put forward a higher demand for time and frequency transfer, which is challenging to be met by the existing GNSS techniques. In this contribution, we presented a new model based on UDUC observations, where the satellite clocks are estimated in the model to avoid the impact of external satellite clock products. In addition, DD ambiguities are formed in the model, which enables high-precision carrier-phase observations to be fully utilized through IAR.

Based on GNSS data from three laboratories, the proposed SCE model was used to evaluate the potential of GNSS time and frequency transfer. In addition, the UDUC

PPP and the SCF models were compared to demonstrate the benefits of IAR and satellite clocks estimation, respectively. According to the experimental results, we found that with IAR, the method using the SCF model improved the precision of time transfer and frequency stability by 20%–50%, showing the benefits of IAR. Furthermore, the SCE model showed a 10%–40% improvement over the SCF model. More importantly, we demonstrated that for averaging times within one day, low-mid 10^{-17} range frequency transfer could be potentially achieved by GPS, Galileo, and BDS-3 once ultra-precise clocks are available.

This study preliminarily proves that GNSS has the potential of reaching picosecond time transfer and sub-10^{-16} frequency transfer, which is expected to be realized with optical clocks. It facilitates our understanding of the advantages of satellite clocks estimation and IAR. However, some theoretical and technical problems, such as expanding the non-common-view model and high-precision atmospheric delay corrections, need to be solved in practice. Our future work will focus on those theoretical and technical problems and continue to explore the improvements and advantages of GNSS for time and frequency transfer.

Acknowledgements This work was partially funded by the Australian Research Council Discovery Project (Grant No. DP 190102444), the National Natural Science Foundation of China (Grant No. 42022025), the Open Fund of Hubei Luojia Laboratory (Grant No. 220100061), and the National Time Service Center, Chinese Academy of Sciences (No. E167SC14). Baocheng Zhang is supported by the CAS Pioneer Hundred Talents Program. We thank PTB and USNO for providing GNSS data. We also thank the IGS for providing precise orbit, clock products and data.

Data availability The datasets generated during the current study are available based on a reasonable request.

Declarations

Conflict of interest All authors declare that they have no conflicts of interest.

References

Boehm J, Werl B, Schuh H (2006) Troposphere mapping functions for GPS and very long baseline interferometry from European Centre for Medium-Range Weather Forecasts operational analysis data. J Geophys Res: Solid Earth 111:2406. https://doi.org/10.1029/2005JB003629

Chen Y, Yuan Y, Zhang B, Liu T, Ding W, Ai Q (2018) A modified mix-differenced approach for estimating multi-GNSS realtime satellite clock offsets. GPS Solut 22:1–10. https://doi.org/10.1007/s10291-018-0739-5

Defraigne P, Aerts W, Harmegnies A, Petit G, Rovera D, Uhrich P (2013) Advances in multi-GNSS time transfer Joint European Frequency and Time Forum & International Frequency Control Symposium. https://doi.org/10.1109/EFTF-IFC.2013.6702126

Defraigne P, Aerts W, Pottiaux E (2015) Monitoring of UTC(k)'s using PPP and IGS realtime products. GPS Solut 19:165–172. https://doi.org/10.1007/s10291-014-0377-5

Defraigne P, Pinat E, Bertrand B, Uhrich P, Chupin B, Riedel F (2021) Stability of hardware delays of GNSS signals. 2021 joint conference of the European frequency and time forum and IEEE international frequency control symposium (EFTF/IFCS). https://doi.org/10.1109/EFTF/IFCS52194.2021.9604324

Delporte J, Mercier F, Laurichesse D, Galy O (2007) Fixing integer ambiguities for GPS carrier phase time transfer. Proceedings of the 2007 IEEE international frequency control symposium-jointly with the 21st European frequency and time forum 1–4:927–932 doi: https://doi.org/10.1109/Freq.2007.4319215

Fujieda M, Piester D, Gotoh T, Becker J, Aida M, Bauch A (2014) Carrier-phase two-way satellite frequency transfer over a very long baseline. Metrologia 51:253. https://doi.org/10.1088/0026-1394/51/3/253

Geng J, Shi C, Ge M, Dodson A, Lou Y, Zhao Q, Liu J (2012) Improving the estimation of fractional-cycle biases for ambiguity resolution in precise point positioning. J Geod 86:579–589. https://doi.org/10.1007/s00190-011-0537-0

Guo J, Geng J (2018) GPS satellite clock determination in case of inter-frequency clock biases for triple-frequency precise point positioning. J Geod 92:1133–1142. https://doi.org/10.1007/s00190-017-1106-y

Guyennon N, Cerretto G, Tavella P, Lahaye F (2009) Further characterization of the time transfer capabilities of precise point positioning (PPP): the sliding batch procedure. IEEE Trans Ultrason Ferroelectr Freq Control 56:1634–1641. https://doi.org/10.1109/Tuffc.2009.1228

Hadas T, Teferle F, Kazmierski K, Hordyniec P, Bosy J (2017) Optimum stochastic modeling for GNSS tropospheric delay estimation in realtime. GPS Solut 21:1069–1081. https://doi.org/10.1007/s10291-016-0595-0

Huang Y, Fujieda M, Takiguchi H, Tseng W, Tsao H (2016) Stability improvement of an operational two-way satellite time and frequency transfer system. Metrologia 53(2):881. https://doi.org/10.1088/0026-1394/53/2/881

Huang G, Zhang Q, Xu G (2014) Realtime clock offset prediction with an improved model. GPS Solut 18:95–104. https://doi.org/10.1007/s10291-013-0313-0

Khodabandeh A, Teunissen P (2016) PPP-RTK and inter-system biases: the ISB look-up table as a means to support multi-system PPP-RTK. J Geod 90:837–851. https://doi.org/10.1007/s00190-016-0914-9

Khodabandeh A, Teunissen P (2018) On the impact of GNSS ambiguity resolution: geometry, ionosphere, time and biases. J Geod 92:637–658. https://doi.org/10.1007/s00190-017-1084-0

Leandro R, Langley R, Santos M (2008) UNB3m_pack: a neutral atmosphere delay package for radiometric space techniques. GPS Solut 12:65–70. https://doi.org/10.1007/s10291-007-0077-5

Liu T, Zhang B (2021) Estimation of code observation-specific biases (OSBs) for the modernized multi-frequency and multi-GNSS signals: an undifferenced and uncombined approach. J Geod 95(8):1–20. https://doi.org/10.1007/s00190-021-01549-x

Liu T, Yuan Y, Zhang B, Wang N, Tan B, Chen Y (2017) Multi-GNSS precise point positioning (MGPPP) using raw observations. J Geod 91:253–268. https://doi.org/10.1007/s00190-016-0960-3

Matsakis D, Defraigne P, Banerjee P (2014) Precise time and frequency transfer. URSI Radio Sci Bull 351:29–44. https://doi.org/10.23919/URSIRSB.2014.7909843

Mi X, Sheng C, El-Mowafy A, Zhang B (2021) Characteristics of receiver-related biases between BDS-3 and BDS-2 for five frequencies including inter-system biases, differential code biases, and differential phase biases. GPS Solut 25:1–11. https://doi.org/10.1007/s10291-021-01151-w

Mi X, Zhang B, Odolinski R, Yuan Y (2020) On the temperature sensitivity of multi-GNSS intra- and inter-system biases and the impact on RTK positioning. GPS Solut 24:1–14. https://doi.org/10.1007/s10291-020-01027-5

Mi X, Zhang B, Yuan Y (2019) Multi-GNSS inter-system biases: estimability analysis and impact on RTK positioning. GPS Solut 23:1–13. https://doi.org/10.1007/s10291-019-0873-8

Nicholson T et al (2015) Systematic evaluation of an atomic clock at 2 x 10 (-18) total uncertainty. Nat Commun 6:1–8. https://doi.org/10.1038/ncomms7896

Odijk D, Khodabandeh A, Nadarajah N, Choudhury M, Zhang B, Li W, Teunissen P (2017) PPP-RTK by means of *S*-system theory: Australian network and user demonstration. J Spat Sci 62:3–27. https://doi.org/10.1080/14498596.2016.1261373

Odijk D, Zhang B, Khodabandeh A, Odolinski R, Teunissen P (2016) On the estimability of parameters in undifferenced, uncombined GN network and PPP-RTK user models by means of *S*-system theory. J Geod 90(1):15–44. https://doi.org/10.1007/s00190-015-0854-9

Odolinski R, Teunissen P, Odijk D (2015) Combined BDS, Galileo, QZSS and GPS single-frequency RTK. GPS Solut 19:151–163. https://doi.org/10.1007/s10291-014-0376-6

Petit G (2021) Sub-10(-16) accuracy GNSS frequency transfer with IPPP. GPS Solut 25:1–9. https://doi.org/10.1007/s10291-020-01062-2

Petit G, Kanj A, Harmegnies A, Loyer S, Delporte J, Mercier F, Perosanz F (2014) GPS frequency transfer with IPPP. 2014 European Frequency and Time Forum (EFTF):451–454. https://doi.org/10.1109/EFTF.2014.7331533

Petit G, Kanj A, Loyer S, Delporte J, Mercier F, Perosanz F (2015) 1 x 10(-16) frequency transfer by GPS PPP with integer ambiguity resolution. Metrologia 52:301–309. https://doi.org/10.1088/0026-1394/52/2/301

Rieck C, Jarlemark P, Jaldehag K, Johansson J (2003) Thermal influence on the receiver chain of GPS carrier phase equipment for time and frequency transfer. IEEE international frequency control symposium and PDA exhibition jointly with the 17th European frequency and time forum. https://doi.org/10.1109/FREQ.2003.1275110

Rose J, Watson R, Allain D, Mitchell C (2014) Ionospheric corrections for GPS time transfer. Radio Sci 49:196–206. https://doi.org/10.1002/2013rs005212

Schuldt T et al (2021) Optical clock technologies for global navigation satellite systems. GPS Solut 25:1–11. https://doi.org/10.1007/s10291-021-01113-2

Shen Y, Li B, Xu G (2009) Simplified equivalent multiple baseline solutions with elevation-dependent weights. GPS Solut 13:165–171. https://doi.org/10.1007/s10291-008-0109-9

Shi C, Guo S, Gu S, Yang X, Gong X, Deng Z, Ge M, Schuh H (2019) Multi-GNSS satellite clock estimation constrained with oscillator noise model in the existence of data discontinuity. J Geod 93:515–528. https://doi.org/10.1007/s00190-018-1178-3

Teunissen P (1995) The least-squares ambiguity decorrelation adjustment: a method for fast GPS integer ambiguity estimation. J Geod 70:65–82. https://doi.org/10.1007/Bf00863419

Teunissen P (1997) On the sensitivity of the location, size and shape of the GPS ambiguity search space to certain changes in the stochastic model. J Geod 71:541–551. https://doi.org/10.1007/s001900050122

Teunissen P (2018) Distributional theory for the DIA method. J Geod 92:59–80. https://doi.org/10.1007/s00190-017-1045-7

Teunissen P (2020) GNSS precise point positioning. Position, navigation, and timing technologies in the 21st Century: integrated satellite navigation. Sensor Syst, Civ Appl 1:503–528. https://doi.org/10.1002/9781119458449.ch20

Teunissen P, Verhagen S (2009) The GNSS ambiguity ratio-test revisited: a better way of using it. Surv Rev 41:138–151. https://doi.org/10.1179/003962609x390058

Tuka A, El-Mowafy A (2013) Performance evaluation of different troposphere delay models and mapping functions. Measurement 46:928–937. https://doi.org/10.1016/j.measurement.2012.10.015

Tu R, Zhang P, Zhang R, Liu J, Lu X (2019) Modeling and performance analysis of precise time transfer based on BDS triple-frequency un-combined observations. J Geod 93:837–847. https://doi.org/10.1007/s00190-018-1206-3

Yao J, Skakun I, Jiang Z, Levine J (2015) A detailed comparison of two continuous GPS carrier-phase time transfer techniques. Metrologia 52:666–676. https://doi.org/10.1088/0026-1394/52/5/666

Yao J, Levine J (2016) A study of GPS carrier-phase time transfer noise based on NIST GPS receivers. J Res Nat Inst Stand Technol 121:372. https://doi.org/10.6028/jres.121.017

Zhang B, Chen Y, Yuan Y (2019) PPP-RTK based on undifferenced and uncombined observations: theoretical and practical aspects. J Geod 93:1011–1024. https://doi.org/10.1007/s00190-018-1220-5

Zhang H, Yuan Y, Li W (2021) An analysis of multisource tropospheric hydrostatic delays and their implications for GPS/GLONASS PPP-based zenith tropospheric delay and height estimations. J Geod 95:1–19. https://doi.org/10.1007/s00190-021-01535-3

Zhang X, Li X, Guo F (2011) Satellite clock estimation at 1 Hz for real-time kinematic PPP applications. GPS Solut 15:315–324. https://doi.org/10.1007/s10291-010-0191-7

Zhang X, Zhang B, Yuan Y, Zha J (2020) Extending multipath hemispherical model to account for time-varying receiver code biases. Adv Space Res 65:650–662. https://doi.org/10.1016/j.asr.2019.11.003

Xiaolong Mi is a Ph.D. candidate at Curtin University and the Innovation Academy for Precision Measurement Science and Technology, Chinese Academy of Sciences. His research focuses on high-precision GNSS positioning, GNSS time and frequency transfer with integer ambiguity resolution, multi-GNSS inter-operability and software development.

Baocheng Zhang is a Professor at the Innovation Academy for Precision Measurement Science and Technology, Chinese Academy of Sciences. His research focuses on modeling multiple global navigation satellite systems for integer ambiguity resolution enabled precise point positioning (PPP-RTK) applications.

Ahmed El-Mowafy is a Professor and Director of Graduate Research, School of Earth and Planetary Sciences, Curtin University, Australia. He obtained his Ph.D. from the University of Calgary, Canada, in 1995 and has more than 200 publications in precise positioning and navigation using GNSS, quality control, POD, integrity monitoring and estimation theory.

Kan Wang is a Professor at the National Time Service Center, Chinese Academy of Sciences. She received her Ph.D. in GNSS advanced modeling from ETH Zurich in 2016 and worked at Curtin University until 2021. Her research interests include high precision GNSS positioning, LEO precise orbit determination, SBAS and integrity monitoring.

Yunbin Yuan is a Professor and the GNSS Application and Research Group director at the Innovation Academy for Precision Measurement Science and Technology, Chinese Academy of Sciences. His current research interests are the following: (1) GNSS-based spatial environmental monitoring and analysis, (2) high-precision GNSS satellite navigation and positioning, and (3) GNSS applications to orbit determination for LEO satellites.